2nd Advanced Optical Metrology Compendium

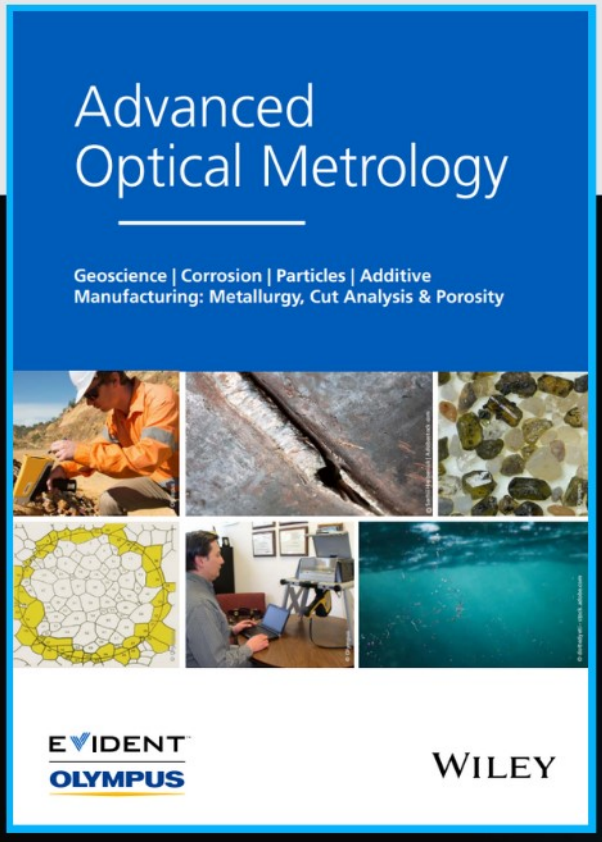

The latest eBook from Advanced Optical Metrology. Download for free.

This compendium includes a collection of optical metrology papers, a repository of teaching materials, and instructions on how to publish scientific achievements.

With the aim of improving communication between fundamental research and industrial applications in the field of optical metrology we have collected and organized existing information and made it more accessible and useful for researchers and practitioners.

EVIDENT
OLYMPUS

WILEY

NANO · MICRO small
www.small-journal.com

Swarming Magnetic Microrobots for Pathogen Isolation from Milk

Carmen C. Mayorga-Martinez, Marketa Castoralova, Jaroslav Zelenka, Tomas Ruml, and Martin Pumera**

Bovine mastitis produced by *Staphylococcus aureus* (*S. aureus*) causes major problems in milk production due to the staphylococcal enterotoxins produced by this bacterium. These enterotoxins are stable and cannot be eradicated easily by common hygienic procedures once they are formed in dairy products. Here, magnetic microrobots (MagRobots) are developed based on paramagnetic hybrid microstructures loaded with IgG from rabbit serum that can bind and isolate *S. aureus* from milk in a concentration of 3.42 10^4 CFU g^{-1} (allowable minimum level established by the United States Food and Drug Administration, FDA). Protein A, which is present on the cell wall of *S. aureus*, selectively binds IgG from rabbit serum and loads the bacteria onto the surface of the MagRobots. The selective isolation of *S. aureus* is confirmed using a mixed suspension of *S. aureus* and *Escherichia coli* (*E. coli*). Moreover, this fuel-free system based on magnetic robots does not affect the natural milk microbiota or add any toxic compound resulting from fuel catalysis. This system can be used to isolate and transport efficiently *S. aureus* and discriminate it from nontarget bacteria for subsequent identification. Finally, this system can be scaled up for industrial use in food production.

1. Introduction

Bovine mastitis is one of the diseases with high economic impact in the world dairy industry and *S. aureus* is the facultative anaerobic Gram-positive coccus responsible for this bovine disease.[1–4] *S. aureus* produce staphylococcal enterotoxins that can cause diarrhea, abdominal cramps, and nausea.[1] Moreover, *S. aureus* can survive pasteurization and thermal sterilization processes, and staphylococcal enterotoxins are stable and cannot be eradicated easily by common hygienic procedures once they are formed in dairy products.[1] For that reason, efficient methods to isolate *S. aureus* bacteria from dairy products for it removal or identification are in high demand and important for the dairy industry.

Several important pathogenic bacteria produce immunoglobulin binding proteins that are thought to help these bacteria evade the host immune response.[5] Examples include protein A of *S. aureus*, protein G of group C and G streptococci, and protein L of *Peptostreptococcus magnus*.[6] Further, immunoglobulin binding proteins have been identified also in mycoplasmas such as *Mycoplasma pneumoniae*[7] and the bovine pathogen *M. bovis*.[8] The ability of these proteins to bind immunoglobulins can be used to selectively bind pathogenic bacteria for their isolation and identification while leaving harmless and beneficial bacteria in solution.

Evolving micro/nanorobots technology justifies expectations to address some unmet biomedical and environmental issues.[9–13] Recently, micro/nanorobots have been used to isolate and eradicate planktonic bacteria[14,15] as well as bacterial biofilms,[16–19] which is important to address the growing risk of pathogen resistance to antibiotics. Moreover, the use of antibiotics to eradicate bacteria in food samples can affect food quality as well as decrease its sensitivity. Micro/nanorobots are able to move using chemical fuels[20,21] or external energy sources (light, magnetic, or ultrasound fields)[22–35] and they can achieve multiple applications, including drug delivery,[36,37] bio/sensing,[38–40] and

C. C. Mayorga-Martinez, M. Pumera
Center for Advanced Functional Nanorobots
Department of Inorganic Chemistry
University of Chemistry and Technology Prague
Technicka 5, 166 28, Czech Republic
E-mail: martin.pumera@ceitec.vutbr.cz

M. Castoralova, J. Zelenka, T. Ruml
Department of Biochemistry and Microbiology
University of Chemistry and Technology Prague
Technicka 5, 166 28, Czech Republic
E-mail: zelenkaa@vscht.cz

The ORCID identification number(s) for the author(s) of this article can be found under https://doi.org/10.1002/smll.202205047.

M. Pumera
Faculty of Electrical Engineering and Computer Science
VSB – Technical University of Ostrava
17. listopadu 2172/15, Ostrava 70800, Czech Republic

M. Pumera
Department of Medical Research
China Medical University Hospital
China Medical University
No. 91 Hsueh-Shih Road, Taichung 40402, Taiwan

M. Pumera
Department of Chemical and Biomolecular Engineering
Yonsei University
50 Yonsei-ro, Seodaemun-gu, Seoul 03722, Korea

DOI: 10.1002/smll.202205047

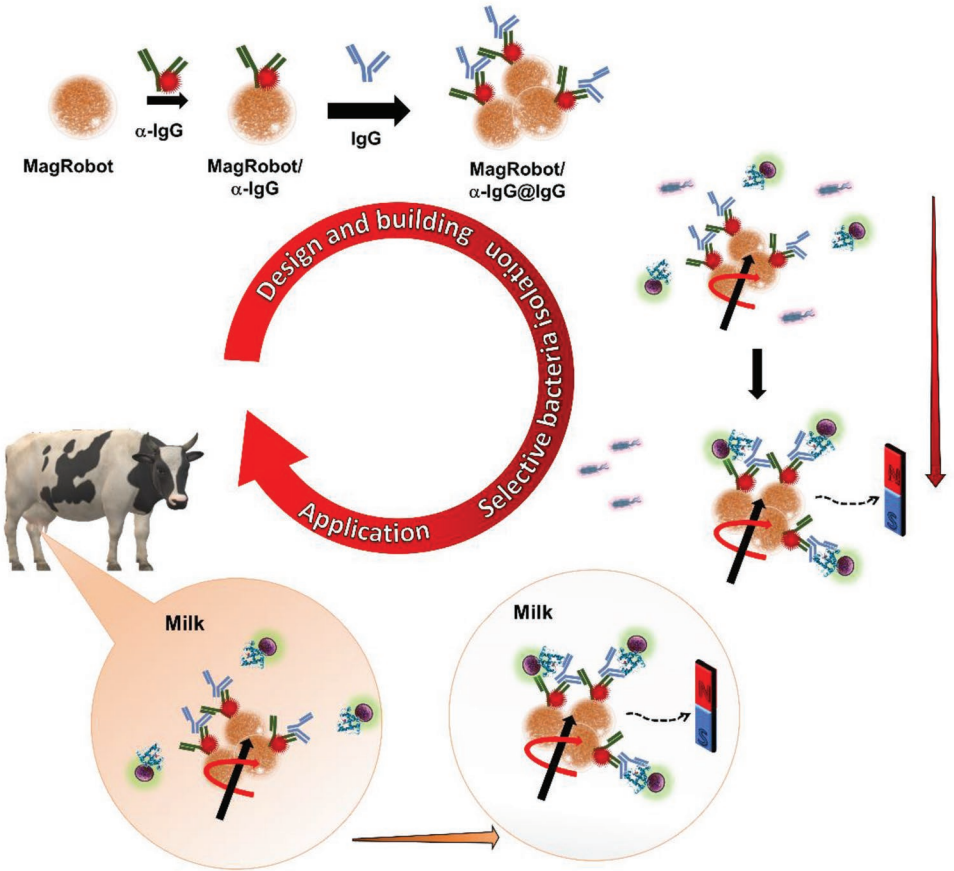

Scheme 1. Schematic representation of *S. aureus* removal by MagRobots. MagRobots were modified with αIgG/RhB@IgG (MagRobots–αIgG/RhB@IgG), which reacts with protein A (top). Protein A is surface-exposed on the *S. aureus* cell wall. After binding on the MagRobots, the *S. aureus* was retrieved by a magnetic field gradient from the suspension containing *E. coli* (right). In addition, MagRobots–αIgG@IgG were used to remove *S. aureus* from milk (bottom).

pathogenic biofilm destroying[15–19] as well as environmental remediation[41–45] and energy harvesting.[46,47] Magnetically propelled micro/nanorobots represent one of the most promising categories that can be used in many applications because they are biocompatible (toxic fuel-free), have strong power propulsion, are remotely maneuverable, and are reconfigurable and programmable.[9,47–49]

Many microrobotic systems have been used to isolate bacteria, spores, and viruses by using various bioreceptors.[12,50–53] Particularly for *S. aureus* isolation, platelets were used as bioreceptors loaded on magnetic and ultrasonic microrobots.[50,51] However, this bioreceptor, although efficient, was not specific.

In this work, we have developed magnetic microrobots that we named "MagRobots," which are able to load, transport, and isolate *S. aureus*. These MagRobots are modified with anti-rabbit IgG produced in goat (αIgG) labeled with rhodamine B (RhB) and IgG from rabbit serum (IgG) (see **Scheme 1**, top). IgG loaded on the MagRobots' surface is specifically bound by the *S. aureus* protein A present on the surface of the *S. aureus* cell wall. Using this approach, *S. aureus* was isolated from the mixture with *E. coli*, which lacks protein A and, therefore, does not bind to the IgG displayed on the MagRobots' surface (see Scheme 1, right). In addition, MagRobots–αIgG/RhB@IgG were used to remove *S. aureus* from milk (Scheme 1, bottom), which is a complex mixture containing also milk microbiota. Moreover, anti-rabbit IgG produced in goat and IgG from rabbit serum are more cost effective than commercially available anti-*S. aureus* antibodies; for scalability of the system, this should also be taken into account. The results obtained in this work, to our knowledge, have not been previously reported.

2. Results and Discussion

Paramagnetic microparticles modified with tosyl (toluenesulfonyl) groups were used to prepare the MagRobots. As can be seen in **Figure 1**A,B, transmission electron microscopy (TEM) images at different magnification reveal the homogeneous size distribution of around 2.8 µm in diameter of MagRobots. In addition, energy-dispersive X-ray spectroscopy (EDS) elemental mapping from TEM images shows the chemical composition of MagRobots; Fe and O confirm the presence of Fe_3O_4 while C and S correspond to tosyl groups (Figure 1C).

Tosyl groups that cover MagRobots allow their conjugation with polyclonal αIgG labeled with RhB (αIgG/RhB) and subsequent loading of IgG from rabbit serum (IgG) (see Scheme 1, top). Serum IgG is bound by protein A, which is exposed on the cell wall of *S. aureus* and allows the MagRobots

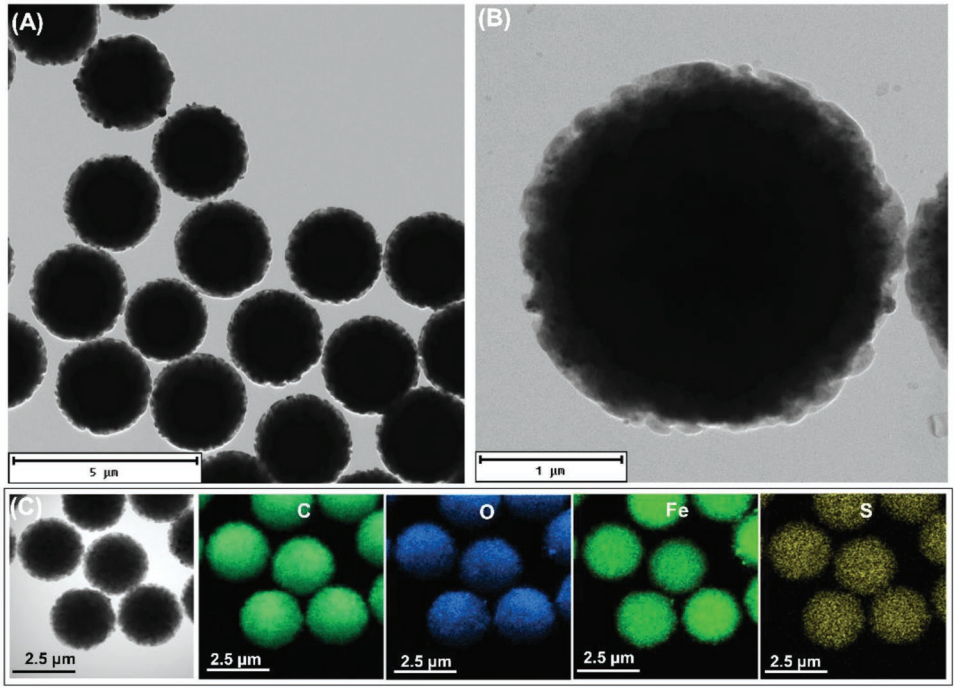

Figure 1. Structural and chemical composition evaluation of MagRobots. A,B) TEM images at different magnification and C) EDS elemental mapping from TEM images of MagRobots.

to load and retrieve the bacteria to clean liquid samples. To confirm that the MagRobots were modified with αIgG, they were inspected by confocal microscopy. For this aim, αIgG/RhB was used as a fluorescent tag. **Figure 2** shows confocal microscopy images of MagRobots with αIgG/RhB and pristine robots used as a control. It can be seen that in the absence of αIgG/RhB, only background auto-fluorescence of pristine microrobots was observed (Figure 2A). This background auto-fluorescence at blue (488 nm) and green excitation (566 nm) is inherent to the tosyl-activated Dynabeads M-280 used in this work.[54–56] However, when microrobots were modified with αIgG/RhB, they showed bright red fluorescence (Figure 2B). After confirming successful modification with αIgG/RhB, the MagRobots were loaded with serum IgG (MagRobots–αIgG/RhB@IgG). The purpose of RhB was to investigate the immobilization of αIgG on the MagRobots' surface as indicated by the fluorescence changing from the faint green auto-fluorescence of pristine MagRobots to the red fluorescence of MagRobots–αIgG/RhB. RhB was only used for surface characterization of the MagRobots and should be omitted in practical applications.

Once successful preparation of the MagRobots–αIgG/RhB@IgG was confirmed, their performance under magnetic actuation was evaluated. MagRobots–αIgG/RhB@IgG were driven by a transversal rotating magnetic field using a homemade 3D-printed 6-coil system adapted to an Olympus inverted microscope table. The magnetic field was applied at intensity of 5 mT. In addition, the magnetic-driven motion of MagRobots–αIgG/RhB@IgG was evaluated in two solutions, PBS/Tween20 (**Figure 3**A) and milk (Figure 3B), and different frequencies applied (Video S1, Supporting Information). As expected, the speed of the MagRobots increased as a function of the frequency applied. This trend is observed in both solutions

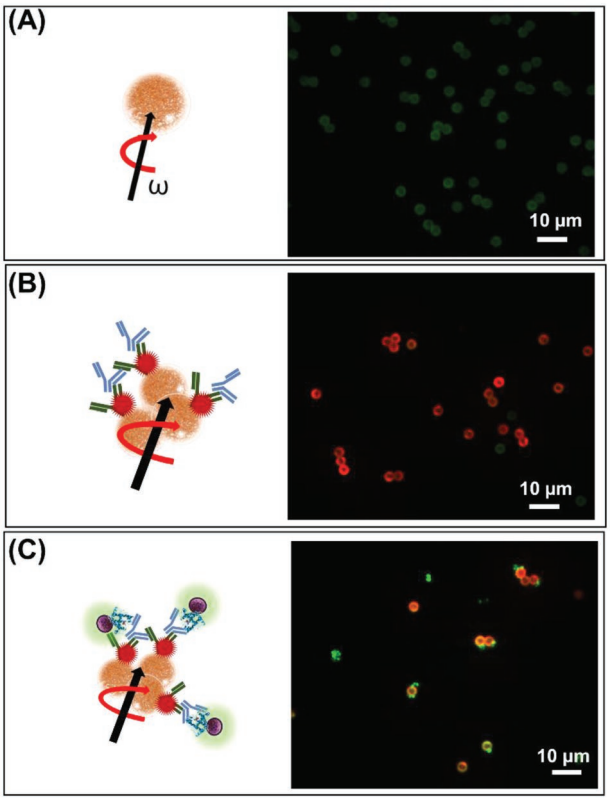

Figure 2. A) Confocal microscopy images of pristine MagRobots. B) MagRobots modified with αIgG/RhB. C) MagRobots modified αIgG/RhB@IgG and *S. aureus* loaded on their surface. *S. aureus* were stained with a SYTO 9 DNA probe. The magnetic actuation conditions for this experiment were 5 Hz, 5 mT, and 1 h under programmed automated motion mode.

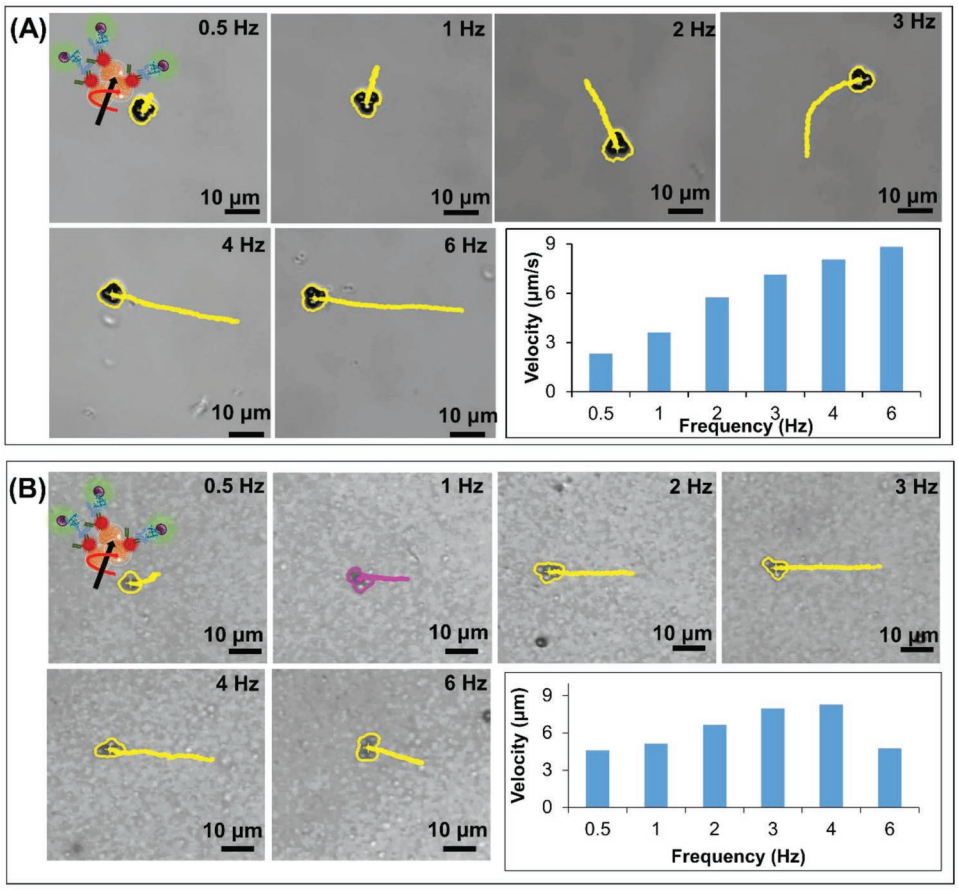

Figure 3. Digital images of MagRobots–αIgG/RhB@IgG under a transversal rotating magnetic field with tracking lines and velocity at different of rotational frequencies in A) PBS/Tween20 and B) milk suspensions. Conditions: 5 mT of magnetic field intensity and tracking lines recorded for 5 s.

(PBS/Tween20 and milk). However, in the presence of milk the MagRobots–αIgG/RhB@IgG move faster but at 6 Hz they lose synchronization and begin to slow down. It appears that the viscosity of milk is favorable to the motion of MagRobots–αIgG/RhB@IgG and there is no need to add any surfactant.

Interestingly, if single paramagnetic particles were driven under a magnetic rotating field in PBS/Tween20 solution, they moved very slowly or remained motionless. The real movement started when at least two particles met and their speed increased as a function of the number of particles (**Figure 4**A). However, the same trend was observed in the suspension of milk but the movement of MagRobots–αIgG/RhB@IgG was faster (Figure 4B). This phenomenon was reported previously by our previous work and by Tasci et al.[38,57]

In addition, to prevent the motion of MagRobots–αIgG/RhB@IgG in only one direction and their accumulation on one side of the test tube, a programmed automated motion mode was used (see Figure 4C,D and Video S2 in the Supporting Information). A predefined rectangular trajectory of MagRobots–αIgG/RhB@IgG under a transversal rotating magnetic field was used to cause MagRobots to "walk" in three rows and two columns, and then return.

After the magnetic actuation of MagRobots–αIgG/RhB@IgG was evaluated, they were placed in a suspension of *S. aureus* (≈10^5 CFU) and a transversal rotating magnetic field applied for 1 h with intensity of 5 mT at 2 Hz. The MagRobots–αIgG/RhB@IgG that load *S. aureus* were retrieved using a permanent magnet. The binding of *S. aureus* to the robots was evaluated by confocal microscopy. Figure 2C shows an overlay of fluorescence signals of MagRobots with red fluorescence and green fluorescence that correspond to αIgG/RhB and *S. aureus* stained with SYTO 9 DNA probe, respectively. In addition, a 3D confocal reconstruction video of MagRobotsαIgG/RhB@IgG alone and bound with *S. aureus* is presented in Video S3 in the Supporting Information. The images clearly show binding of *S. aureus* onto the MagRobots–αIgG/RhB @IgG.

In addition, we made a video of MagRobots–αIgG/RhB@IgG propelled in a suspension of *S. aureus* by transversal rotating magnetic field with intensity of 5 mT at 2 Hz. Video S4 in the Supporting Information was recorded immediately after MagRobots–αIgG/RhB@IgG were placed in the *S. aureus* suspension. Initially, isolated particles were observed, but when the transversal rotating magnetic field was applied, they started to form chains and move faster, and for longer distances (Video S4, left panel, Supporting Information). The chains did not disassemble after switching off the transversal rotating magnetic field (Video S4, right panel, Supporting Information). After 5 min, the MagRobots–αIgG/RhB@IgG chains loaded visible amounts of *S. aureus* as seen in Video S5 (Supporting Information), which was recorded at magnetic field intensity of 5 mT at 2 Hz.

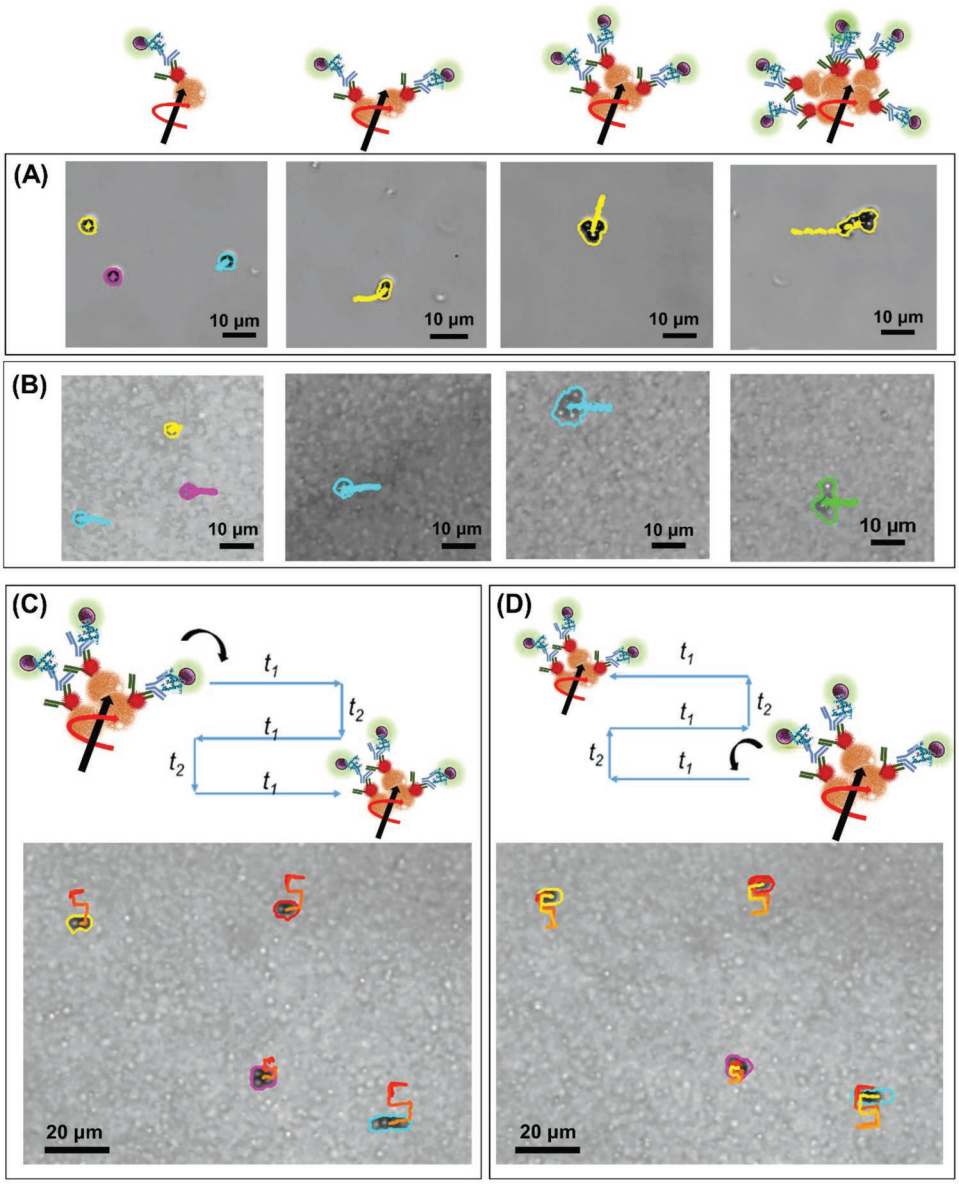

Figure 4. Digital images of MagRobots–αIgG/RhB@IgG under a transversal rotating magnetic field with tracking lines at 5 Hz in A) PBS/Tween20 and B) milk suspensions. In these experiments, MagRobots comprising 1, 2, 3, or multiple particles were compared. Digital images of MagRobots–αIgG/RhB@IgG under a transversal rotating magnetic field with tracking lines at 5 Hz and using programmed automated motion mode in milk suspension. In this programmed automated mode, MagRobots–αIgG/RhB@IgG "walk" in C) three rows and two columns and D) return. Conditions: 5 mT of magnetic field intensity.

Once the loading and retrieval of *S. aureus* by MagRobots–αIgG/RhB@IgG were confirmed, the efficiency of *S. aureus* removal was evaluated by quantification of bacteria in the robots-treated suspension using a cultivation method (see details in the Experimental Section). **Figure 5**A summarizes the percentage of relative number of viable bacteria of *S. aureus* remaining in the solution after their retrieval using MagRobots–αIgG/RhB@IgG (red column) and not IgG-coated on MagRobots (blue column). Clearly, it can be seen that MagRobots–αIgG/RhB@IgG were able to remove ≈60% of *S. aureus* cells in 1 h, whereas the control MagRobots did not remove any bacteria as indicated by the ≈100% relative number of viable bacteria compared to the bacterial concentration in the original solution (see black column). In addition, we have evaluated bacteria removal using MagRobots of various sizes with diameters of 1, 2.8, and 5 μm (see Figure 5B). MagRobots of diameter 5 μm almost failed to bind *S. aureus* as documented by removal of only ≈2% (Figure 5B, orange column) followed by the 1 μm MagRobots that removed ≈35% of *S. aureus* (Figure 5B, green column). In contrast, 2.8 μm MagRobots removed ≈60% of bacteria (Figure 5B, red column). Therefore, for the following experiment, 2.8 μm MagRobots were used. The most plausible reason for the poor performance of 5 μm MagRobots is that the amount of αIgG used was not sufficient

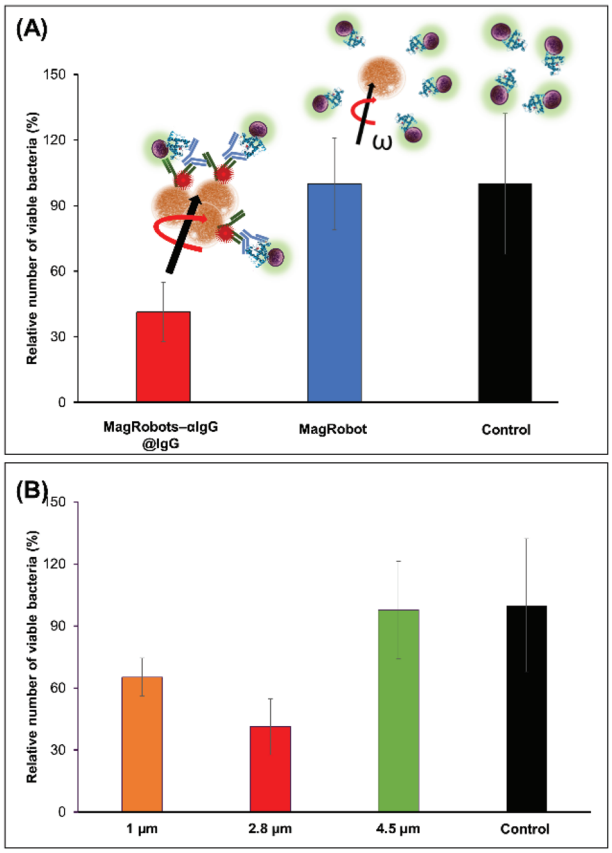

Figure 5. A) Relative number of viable bacteria after *S. aureus* retrieval using MagRobots either modified or not modified with αIgG/RhB@IgG. B) Relative number of viable bacteria after *S. aureus* retrieval using MagRobots with different diameters (1, 2.8, and 5 μm) modified with αIgG/RhB@IgG. Magnetic actuation conditions: 5 Hz, 5 mT, and 1 h under programmed automated motion mode. Values are the average of three independent measurements performed in triplicate. Data are displayed as mean ± SD.

to modify their surface and, in consequence, bovine serum albumin (BSA) blocked their surface and IgG was not loaded efficiently to isolate *S. aureus*.

To prove the selective retrieval of *S. aureus* (i.e., bacteria that produce immunoglobulin binding protein A), MagRobots–αIgG/RhB@IgG were mixed with *E. coli* (bacteria that does not produce immunoglobulin binding protein) and confocal microscopy images were taken. *Staphylococcus aureus* and *E. coli* cells were at the same concentration. **Figure 6**A shows clearly that *E. coli* did not attach to the surface of MagRobots–αIgG/RhB@IgG as only *S. aureus* was observed on the robots despite the presence of both bacteria in the solution (Figure 6B). This confirms the selectivity of the interaction of IgG with the protein A exposed on the cell wall of *S. aureus*.

In addition, the selective *S. aureus* retrieval by MagRobots-modified αIgG/RhB@IgG was evaluated by the quantification of bacteria using a cultivation method (see the Experimental Section for details). For this aim, MagRobots/anti-IgG@RhB/IgG were placed in a mixed suspension of both bacteria. After 1 h of applying a transversal rotating magnetic field, the bacteria attached to MagRobots were retrieved using a permanent magnet and the bacteria remaining in the sample were quantified. Figure 6C shows digital photographs of one droplet of bacterial solution cultivated overnight before and after treatment with MagRobots–αIgG/RhB@IgG. The left panel shows colony-forming units of *E. coli* (big dots) and *S. aureus* (small dots) grown from inoculum from an untreated bacterial suspension. The photograph in the right panel shows one drop of the solution remaining after the bacteria retrieval. Clearly, it can be seen that the number of *E. coli* colonies is similar in the untreated (Figure 6C, left panel) and treated bacterial suspensions (Figure 6C, right panel). However, the number of *S. aureus* colonies decreased significantly upon treatment with the MagRobots–αIgG/RhB@IgG and the robots' subsequent retrieval using a permanent magnet (Figure 6C, right panel). The same results were observed by quantification of the relative number of bacteria of *E. coli* and *S. aureus* before and after they were treated with MagRobots–αIgG/RhB@IgG (Figure 6D). Blue and red columns correspond to the relative number of viable *E. coli* and *S. aureus*, respectively, before (columns with patter fill) and after (columns with solid fill) treatment with MagRobots–αIgG/RhB@IgG. Viable *S. aureus* cells decreased by 50% after their removal by MagRobots–αIgG/RhB@IgG. In addition, when applying the *t*-test statistical analysis with a confidence interval of 95%, the mean values for the relative number of viable *E. coli* after and before treatment with MagRobots were not statistically different with $p = 0.4199$, whereas the mean values for the relative number of viable *S. aureus* after and before treatment with MagRobots were statistically different with $p = 0.0329$ and a confidence interval of 95%. Additional experiments to ensure the selectivity of MagRobots–αIgG/RhB@IgG were performed using *Lactobacillus rhamnosus* (*L. rhamnosus*) and *Enterobacter cloacae* (*E. cloacae*) (see Figure S1 in the Supporting Information). In both cases, no significant differences in the number of viable bacteria before and after treatment with MagRobots–αIgG/RhB@IgG were observed.

Next, we investigated the effect of different concentrations of IgG used to prepare MagRobots–αIgG/RhB@IgG. For this aim, two concentrations of IgG were used: 5 and 10 μg mL^{-1}. **Figure 7**A shows that 10 μg mL^{-1} of IgG applied onto MagRobots–αIgG/RhB@IgG can effectively remove ≈75% of *S. aureus*, whereas 5 μg mL^{-1} MagRobots–αIgG/RhB@IgG removed ≈60% of *S. aureus*. In both cases, 60 min were needed to remove *S. aureus*. Following the effective removal of *S. aureus* using MagRobots–αIgG/RhB@IgG, their propulsion effect on *S. aureus* removal was evaluated (Figure 7B). Immotile (static mode) MagRobots–αIgG/RhB@IgG (ordinary magnetic separation) can remove around 37% of *S. aureus* cells while propelled MagRobots–αIgG/RhB@IgG (dynamic mode) are capable of removing twice as many bacteria (75.4%). This result demonstrates the importance of the MagRobots' mobility in removing *S. aureus* from a bacterial suspension.

The magnetic separation for bacterial separation and subsequent identification, quantification, or removal is a well-known methodology.[58,59] However, in this case, the microparticles are static or need an external shaker; hence, its implementation in milk factory pipelines is not practical.

Each MagRobots–αIgG/RhB@IgG component is scrutinized to understand and affirm their role (Figure 7C). Bare MagRobots were not able to remove *S. aureus* (blue column), whereas

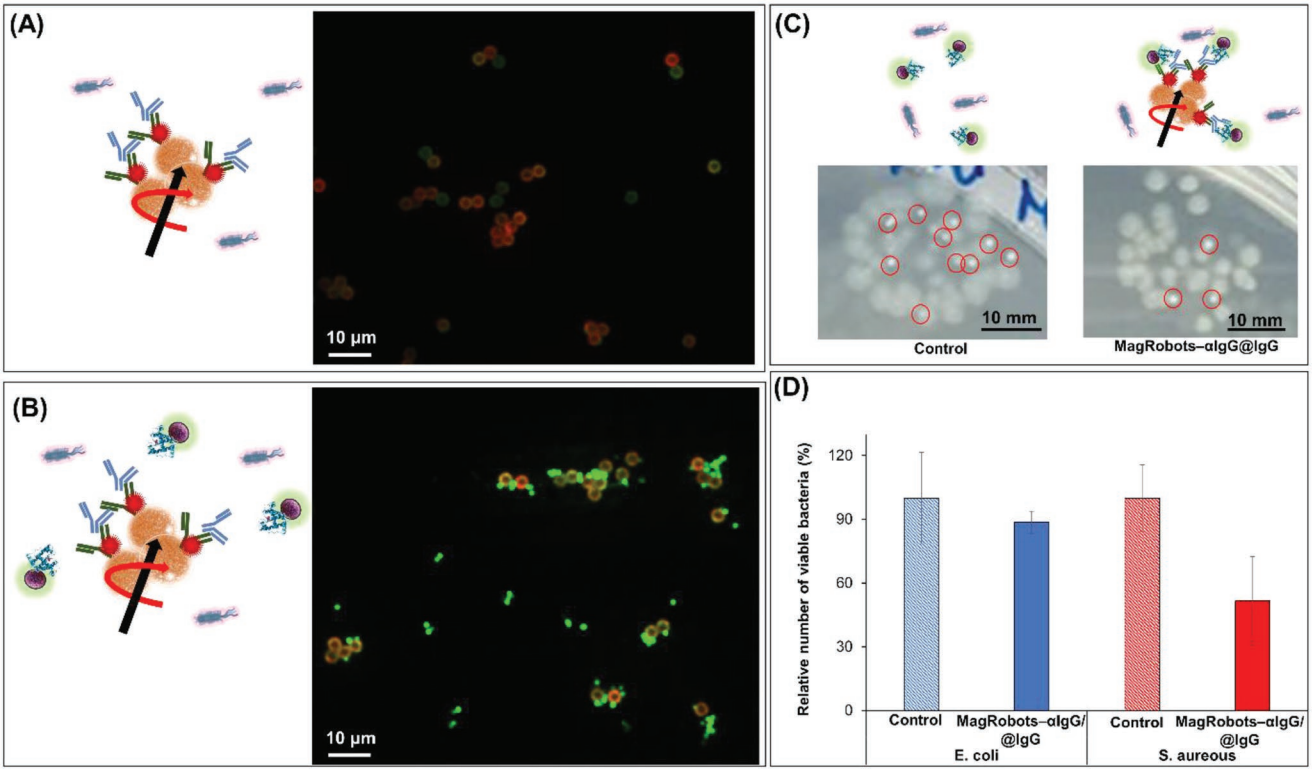

Figure 6. Confocal microscopy images of A) MagRobots–αIgG/RhB@IgG in the presence of *E. coli* and B) selective *S. aureus* retrieval from its mixture with *E. coli* by MagRobots–αIgG/RhB@IgG. Bacteria were stained with SYTO 9 DNA probe. Selective *S. aureus* retrieval by MagRobots–αIgG/RhB@IgG in the presence of *E. coli*. C) Digital photographs of colony-forming units and D) percentage of relative number of viable bacteria in the bacterial mixture (*S. aureus* and *E. coli*) before and after treatment using MagRobots–αIgG/RhB@IgG. Magnetic actuation conditions: 5 Hz, 5 mT, and 1 h under programmed automated motion mode. Values are the average of three independent measurements performed in triplicate. Data are displayed as mean ± SD.

MagRobots–αIgG/RhB@IgG were able to remove around 64% of *S. aureus* (red column). However, MagRobots–αIgG/RhB@IgG with anti-IgG antibody enhanced *S. aureus* removal. We suggest that the enhancement is due to the possibility to load more IgG on the surface of the MagRobots using the primarily bound anti-IgG (αIgG).

An additional experiment was performed using lower concentration of *S. aureus* and the same concentration of MagRobots–αIgG/RhB@IgG. The result is shown in Figure 7D, when the initial concentration of *S. aureus* (about 10^4 CFU) was reduced by 98%. Moreover, the effect of different MagRobot speeds was evaluated at different frequencies (see Figure S2 in the Supporting Information). The relative number of viable bacteria slightly increased as the frequency decreased, indicating that MagRobots–αIgG/RhB@IgG speed affects in some way the efficiency of bacteria isolation.

Finally, *S. aureus* removal from milk samples using MagRobots–αIgG/RhB@IgG and under a transversal rotating magnetic field was evaluated. In this experiment, pasteurized milk samples were spiked with *S. aureus* bacteria with a concentration of about 10^4 CFU. Then, MagRobots–αIgG/RhB@IgG were placed in the milk with *S. aureus* samples and a transversal rotating magnetic field applied with intensity of 5 mT at 2 Hz for 1 h under programmed automated motion mode. The MagRobots–αIgG/RhB@IgG were then retrieved using a magnetic field gradient and the remaining *S. aureus* in milk samples were quantified. As can be seen in **Figure 8**, the motors were able to isolate efficiently around 83% of *S. aureus* present in the milk samples.

Low levels of *S. aureus* may be found in raw milk even when produced using good manufacturing practices. Furthermore, the pasteurization process does not kill efficiently *S. aureus* bacteria.[60] According to FDA guidance,[61] excessive numbers of *S. aureus* in raw milk or other dairy products, i.e., greater than or equal to 10^4 colony forming units per gram (cfu g^{-1}) indicates that the product was produced under unsanitary conditions. MagRobots–αIgG/RhB@IgG developed here were able to remove 3.42 10^4 cfu g^{-1} of *S. aureus*. In consequence, these results indicate that our system can successfully remove *S. aureus* remaining after the milk has been pasteurized. Moreover, this fuel-free removal system based on magnetic robots is specific to *S. aureus* bacteria and does not affect the natural milk microbiota or add toxic compounds resulting from fuel catalysis. To the best of our knowledge, no similar results have been published before using microrobot technology.

In addition, to evaluate the safety of MagRobots used in this application, an in vitro cytotoxicity assay was carried out in two cell lines (HeLa and MRC). Pristine MagRobots and MagRobots modified with αIgG/RhB@IgG at seven concentrations were exposed for 1 and 48 h. After these times, cytotoxicity was evaluated using a resazurin method assay. Figure S3 in the Supporting Information shows the toxicological profiles that

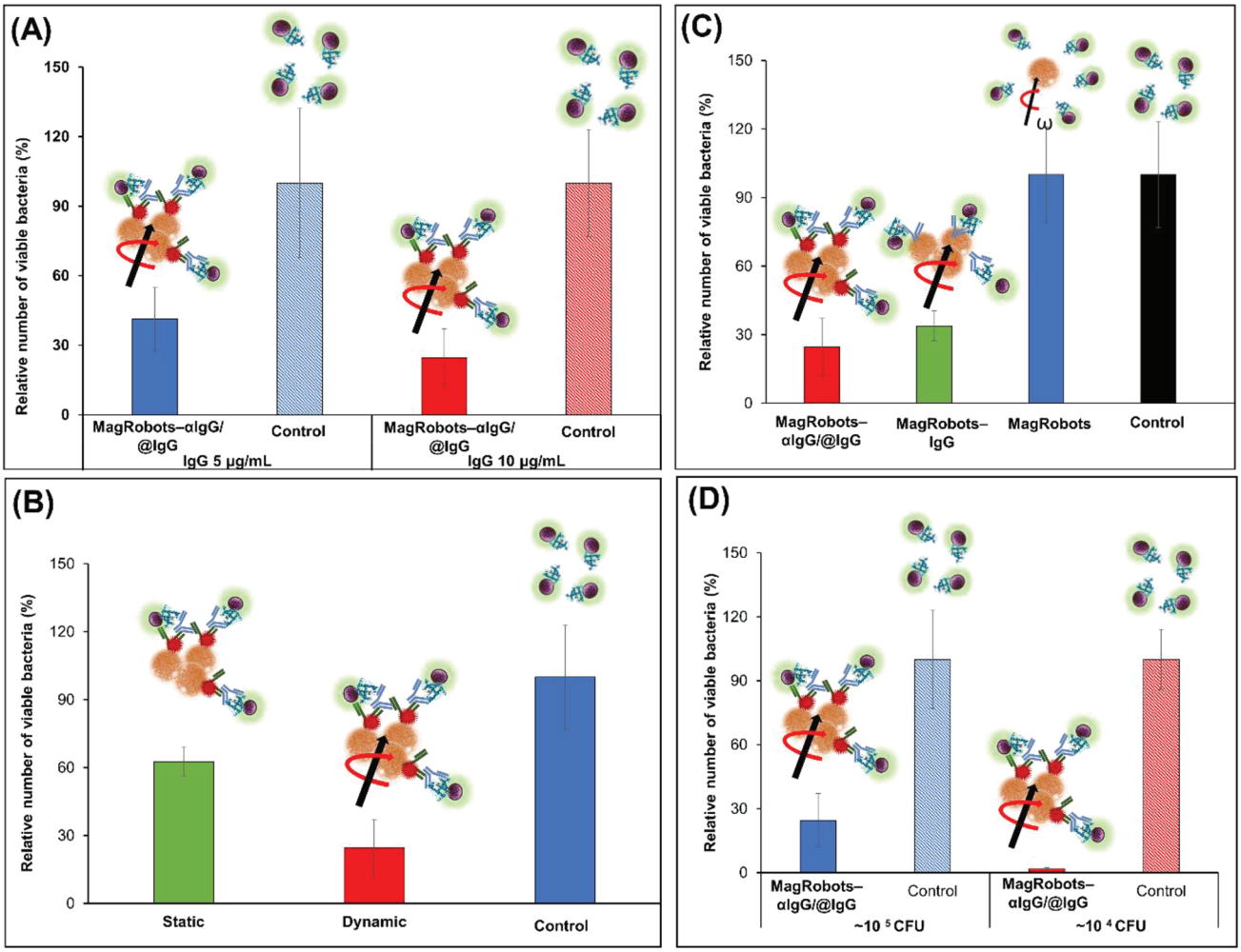

Figure 7. A) *Staphylococcus aureus* removal efficiency evaluation by MagRobots–αIgG/RhB@IgG prepared using different concentrations of IgG. B) *Staphylococcus aureus* removal efficiency using MagRobots–αIgG/RhB@IgG in static and dynamic modes. C) Evaluation of the role of each MagRobots–αIgG/RhB@IgG component in the efficient removal of *S. aureus*. D) *Staphylococcus aureus* removal at different bacterial concentrations. Magnetic actuation conditions: 5 Hz, 5 mT, and 1 h under programmed automated motion mode. Values are the average of three independent measurements performed in triplicate. Data are displayed as mean ± SD.

indicate that the cell viability expressed as metabolic activity was not affected upon the introduction of MagRobots in all concentrations tested.

The performance of MagRobots–αIgG/RhB@IgG in terms of bacteria isolation efficiency and time employed to do it was compared with previous reports where different robots modified with different receptors were able to remove bacteria, spores, and pseudo-viruses (see Table S1 in the Supporting Information).[12,49–52] In terms of isolation time, MagRobots–αIgG/RhB@IgG showed similar performance with catalytic micromotors used to isolate *B. globigii* spores[51] and better than the algae-robots used to isolate SARSCoV-2 pseudo-virus.[52] However, catalytic micromotors and algae-robots lack propulsion control because they are self-propelled by chemical fuel and their intrinsic mobility, respectively. This fact makes microorganism retrieval difficult in real applications because the motors/robots must be separated by centrifugation. Moreover, catalytic micromotors move by using a high concentration of toxic H_2O_2.[12,51] In addition, the isolation time of MagRobots–αIgG/RhB@IgG was worse than for helical nanomotors and gold nanowires propelled by rotating magnetic field and ultrasound.[49,50] Nevertheless, helical nanomotors and gold nanowires use platelets as receptors, which lack specificity. Finally the isolation efficiency was similar in all cases (see Table S1 in the Supporting Information).

3. Conclusion

We developed magnetic microrobots capable of the efficient and specific removal of *S. aureus* (as a representative of bacteria that produce immunoglobulin binding proteins) from liquid samples. These MagRobots were modified with anti-rabbit IgG produced in goat and IgG from rabbit serum. Protein A, which is present on the cell wall of *S. aureus*, binds IgG and loads the bacterial cells onto the surface of the MagRobots. The selective removal of *S. aureus* by MagRobots–αIgG/RhB@IgG was evaluated using *E. coli* as the negative control. A mixture of both

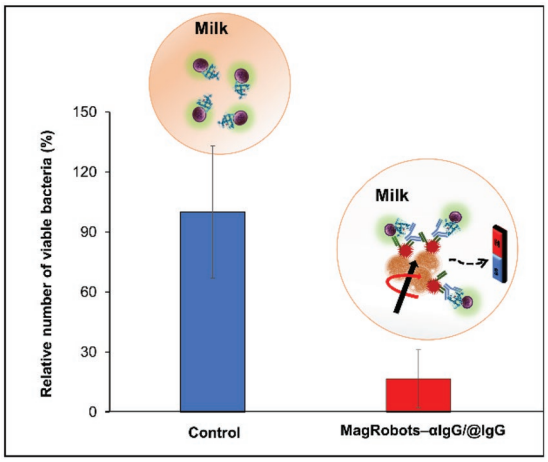

Figure 8. *Staphylococcus aureus* removal from milk using MagRobots–αIgG/RhB@IgG. Magnetic actuation conditions: 5 Hz, 5 mT, and 1 h under programmed automated motion mode. Values are the average of three independent measurements performed in triplicate. Data are displayed as mean ± SD.

bacteria (*S. aureus* and *E. coli*) was treated with MagRobots–αIgG/RhB@IgG and it was proved that these MagRobots were able to remove specifically *S. aureus*. Overall, surface modification of the micro/nanorobots used in this work could be used to remove not only *S. aureus* but also other bacteria that produce immunoglobulin binding proteins. Indeed, surface modification of the micro/nanorobots by antibodies against specific surface proteins of pathogenic bacteria offers an attractive strategy for the targeted removal of a variety of pathogens. In addition, MagRobots–αIgG/RhB@IgG were used to remove *S. aureus* from a dairy product (milk). The removal of *S. aureus* from dairy products is a challenge because this bacterium can survive the pasteurization process and the use of antibiotics can compromise the quality of the food. MagRobots–αIgG/RhB@IgG offer a promising alternative to removing bacteria in the dairy products industry. However, this research is a proof-of-concept where the experiments were done in laboratory-scale using expensive commercial reagents. In the case of real and large-scale applications, the cost of the motors can be very low as the MagRobots are based on Fe_3O_4 and polymers. Also, it should be noted that these MagRobots can enter hard-to-reach places within a milk production plant and operate wirelessly. Finally, these motors can remove bacteria and also specifically isolate *S. aureus* for their subsequent determination and quantification.

4. Experimental Section

Magnetic Drive of MagRobots: Videos were recorded using a Basler acA-1920-155 µm monochrome CMOS camera and homemade 3D-printed 6-coil system adapted to an Olympus inverted microscope table with a 50× objective lens. MagRobots–αIgG/RhB@IgG were placed inside the 6-coil system and a transversal rotating magnetic field applied at intensity of 5 mT.

MagRobot Modification with Immunoassay and S. aureus Isolation: 3 mg mL^{-1} of MagRobots (Dynabeads M-280 tosyl-activated from Invitrogen, Czech Republic) were conjugated overnight with 40 ng mL^{-1} polyclonal anti-rabbit IgG produced in goat and fluorescence labeled with rhodamine B (Invitrogen, Czech Republic) at 37 °C with continuous agitation at 400 rpm. Before this conjugation step, they were washed twice in borate buffer of pH 9.2. After, the resulted solution was washed with PBS pH 7.4 prepared from tablet (Sigma-Aldrich, Czech Republic) and 0.5% Tween 20 (Sigma-Aldrich, Czech Republic). Then, the free spaces of MagRobots were blocked with 5% BSA (Sigma-Aldrich, Czech Republic) solution in PBS for 1 h at 25 °C (400 rpm) followed by washing using 1% BSA in PBS solution. Finally, the modified MagRobots/anti-IgG were incubated with IgG from rabbit serum (Sigma-Aldrich, Czech Republic) at desired concentration to obtain MagRobots/anti-IgG/IgG followed by washing with PBS/0.5% Tween 20. Next, MagRobots/anti-IgG/IgG were placed in a bacterial solution (≈10^5 CFU) and a transversal rotating magnetic field applied with intensity of 5 mT and 5 Hz for 30 min under circular predefined motion.

Bacterial Strains, Cultivation, and Preparation of Bacterial Solutions: The bacteria, *Staphylococcus aureus* (CCM3953) and *Escherichia coli* (DBM 313), were cultivated overnight in Luria–Bertani (LB) broth (Sigma-Aldrich, L3022, USA) at 37 °C, 150 rpm. The overnight cultures were diluted by sterile PBS to match the optical density of a 1.0 McFarland (≈10^8 CFU) standard (Densilameter II, Erba Mannheim, Germany). The prepared bacterial suspension was either used directly or further diluted by sterile PBS using decimal dilution. To prepare milk samples spiked with *S. aureus*, pasteurized milk was purchased from a local supermarket and used instead of PBS.

Drop-Plate Method for Enumerating Bacteria: After the retrieval of bacteria from the suspension using MagRobots/anti-IgG/IgG, the bacteria remaining in the suspension were enumerated using the drop-plate method. The suspensions were decimally diluted in PBS and 20 µL of the prepared diluted suspensions were dropped (three times) on the Plate Count Agar (PCA) plates (Oxoid, UK). After incubation of the plates overnight at 37 °C, the colonies (*S. aureus* and *E. coli*) within the drops were counted to estimate the number of CFUs for each bacterium.

Confocal 3D Microscopy: Confocal 3D images were recorded using an Andor revolutionxD system on an Olympus IX81 microscope operated with iQ3software. Bacterial cells were stained with SYTO 9 DNA probe.

Cytotoxicity Assay: Cells were cultured in EMEM medium with 5% fetal bovine serum. Cell viability was evaluated by resazurin assay (Alamar Blue) and visually confirmed by microscopic inspection.

Statistical Analysis: In all experiments, values are the average of three independent measurements and data are displayed as mean ± standard deviation (SD). Data were processed using Microsoft Excel software. T-test statistical analysis was made with a confidence interval of 95%.

Supporting Information

Supporting Information is available from the Wiley Online Library or from the author.

Acknowledgements

This work was supported by the project "Advanced Functional Nanorobots" (Reg. No. CZ.02.1.01/0.0/0.0/15_003/0000444 financed by the EFRR).

Conflict of Interest

The authors declare no conflict of interest.

Data Availability Statement

The data that support the findings of this study are available from the corresponding author upon reasonable request.

Keywords

bacteria, collective behavior, infections, micromachines

Received: August 17, 2022
Revised: November 1, 2022
Published online:

[1] J. Kümmel, B. Stessl, M. Gonano, G. Walcher, O. Bereuter, M. Fricker, T. Grunert, M. Wagner, M. Ehling-Schulz, *Front Microbiol* **2016**, *7*, 1603.
[2] J. Romero, E. Benavides, C. Meza, *Front Vet Sci* **2018**, *5*, 273.
[3] Y. Ayele, F. D. Gutema, B. M. Edao, R. Girma, T. B. Tufa, T. J. Beyene, F. Tadesse, M. Geloye, A. F. Beyi, *BMC Microbiol.* **2017**, *17*, 141.
[4] K. Artursson, M. Nilsson-Öst, K. P. Waller, *J. Dairy Sci.* **2010**, *93*, 1534.
[5] J. M. Woof, *Biochem. Soc. Trans.* **2016**, *44*, 1651.
[6] M. Graille, E. A. Stura, N. G. Housden, J. A. Beckingham, S. P. Bottomley, D. Beale, M. J. Taussig, B. J. Sutton, M. G. Gore, J. B. Charbonnier, *Structure* **2001**, *9*, 679.
[7] C. Blötz, N. Singh, R. Dumke, J. Stülke, *Front. Microbiol.* **2020**, *11*, 685.
[8] H. Zhao, Y. Zhang, Z. Wang, M. Liu, P. Wang, W. Wu, C. Peng, *Front. Vet. Sci.* **2021**, *8*, 644224.
[9] H. Zhou, C. C. Mayorga-Martinez, S. Pané, L. Zhang, M. Pumera, *Chem. Rev.* **2021**, *121*, 4999.
[10] F. Soto, E. Karshalev, F. Zhang, B. E. Fernandez de Avila, A. Nourhani, J. Wang, *Chem. Rev.* **2022**, *122*, 5365.
[11] B. Jurado-Sánchez, A. Escarpa, *Trends Anal. Chem.* **2016**, *84*, 48.
[12] J. Gao, K. Yuan, L. Zhang, *Field-Driven Micro and Nanorobots for Biology and Medicine* (Eds: Y. Sun, X. Wang, J. Yu), Springer, Cham **2022**.
[13] S. Campuzano, J. Orozco, D. Kagan, M. Guix, W. Gao, S. Sattayasamitsathit, J. C. Claussen, A. Merkoçi, J. Wang, *Nano Lett.* **2012**, *12*, 396.
[14] B. E. F. de Ávila, P. Angsantikul, J. Li, M. A. Lopez-Ramirez, D. E. Ramírez-Herrera, S. Thamphiwatana, C. Chen, J. Delezuk, R. Samakapiruk, V. Ramez, M. Obonyo, L. Zhang, J. Wang, *Nat. Commun.* **2017**, *8*, 272.
[15] C. C. Mayorga-Martinez, J. Zelenka, J. Grmela, H. Michalkova, T. Ruml, J. Mareš, M. Pumera, *Adv. Sci.* **2021**, *8*, 2101301.
[16] Y. Dong, L. Wang, K. Yuan, F. Ji, J. Gao, Z. Zhang, X. Du, Y. Tian, Q. Wang, L. Zhang, *ACS Nano* **2021**, *15*, 5056.
[17] G. Hwang, A. J. Paula, E. E. Hunter, Y. Liu, A. Babeer, B. Karabucak, K. Stebe, V. Kumar, E. Steager, H. Koo, *Sci. Robot.* **2019**, *4*, eaaw2388.
[18] C. C. Mayorga-Martinez, J. Zelenka, K. Klima, P. Mayorga-Burrezo, L. Hoang, T. Ruml, M. Pumera, *ACS Nano* **2022**, *16*, 8694.
[19] Z. Zhang, L. Wang, T. K. F. Chan, Z. Chen, M. Ip, K. S. Chan Paul, J. J. Y. Sung, L. Zhang, *Adv. Healthcare Mater.* **2022**, *11*, 2101991.
[20] R. Mundaca-Uribe, B. Esteban-Fernández de Ávila, M. Holay, L. P. Venugopalan, B. Nguyen, J. Zhou, J. A. Abbas, R. H. Fang, L. Zhang, J. Wang, *Adv. Healthcare Mater.* **2020**, *9*, 2000900.
[21] Solovev, A. A. , Mei, Y. , Ureña, E. B. , Huang, G. , SchmidtO. G , *Small* **2009**, *5*, 1688.
[22] W. Gao, S. Sattayasamitsathit, J. Orozco, J. Wang, *J. Am. Chem. Soc.* **2011**, *133*, 11862.
[23] L. Kong, C. C. Mayorga-Martinez, J. Guan, M. Pumera, *ACS Appl. Mater. Interfaces* **2018**, *10*, 22427.
[24] L. Xu, F. Mou, H. Gong, M. Luo, J. Guan, *Chem. Soc. Rev.* **2017**, *46*, 6905.
[25] F. Mou, L. Kong, C. Chen, Z. Chen, L. Xu, J. Guan, *Nanoscale* **2016**, *8*, 4976.
[26] J. Llacer-Wintle, A. Rivas-Dapena, X.-Z. Chen, E. Pellicer, B. J. Nelson, J. Puigmartí-Luis, S. Pané, *Adv. Mater.* **2021**, *33*, 2102049.
[27] J. Wu, B. Jang, Y. Harduf, Z. Chapnik, Ö. B. Avci, X. Chen, J. Puigmartí-Luis, O. Ergeneman, B. J. Nelson, Y. Or, S. Pané, *Adv. Sci.* **2021**, *8*, 2004458.
[28] J. M. McNeill, N. Nama, J. M. Braxton, T. E. Mallouk, *ACS Nano* **2020**, *14*, 7520.
[29] S. Sabrina, M. Tasinkevych, S. Ahmed, A. M. Brooks, M. Olvera de la Cruz, T. E. Mallouk, K. J. M. Bishop, *ACS Nano* **2018**, *12*, 2939.
[30] J. Li, C. C. Mayorga-Martinez, C. D. Ohl, M. Pumera, *Adv. Funct. Mater.* **2022**, *32*, 2102265.
[31] W. Gao, D. Kagan, O. S. Pak, C. Clawson, S. Campuzano, E. Chuluun-Erdene, E. Shipton, E. E. Fullerton, L. Zhang, E. Lauga, J. Wang, L. Zhang, *Small* **2012**, *8*, 460.
[32] W. Gao, S. Sattayasamitsathit, K. M. Manesh, D. Weihs, J. Wang, *J. Am. Chem. Soc.* **2010**, *132*, 14403.
[33] V. Garcia-Gradilla, J. Orozco, S. Sattayasamitsathit, F. Soto, F. Kuralay, A. Pourazary, A. Katzenberg, W. Gao, Y. Shen, J. Wang, *ACS Nano* **2013**, *7*, 9232.
[34] W. Gao, X. Feng, A. Pei, C. R. Kane, R. Tam, C. Hennessy, J. Wang, *Nano Lett.* **2014**, *14*, 305.
[35] J. Li, T. Li, T. Xu, M. Kiristi, W. Liu, Z. Wu, J. Wang, *Nano Lett.* **2015**, *15*, 4814.
[36] M. Pacheco, C. C. Mayorga-Martinez, J. Viktorova, T. Ruml, A. Escarpa, M. Pumera, *Appl. Mater. Today* **2022**, *27*, 101494.
[37] R. Mundaca-Uribe, E. Karshalev, B. Esteban-Fernández de Ávila, X. Wei, B. Nguyen, I. Litvan, R. H. Fang, L. Zhang, J. Wang, *Adv. Sci.* **2021**, *8*, 2100389.
[38] C. C. Mayorga-Martinez, J. Vyskočil, F. Novotný, P. Bednar, D. Ruzek, M. Pumera, *Appl. Mater. Today* **2022**, *26*, 101337.
[39] J. Kim, C. C. Mayorga-Martinez, J. Vyskočil, D. Ruzek, M. Pumera, *Appl. Mater. Today* **2022**, *27*, 101402.
[40] R. María-Hormigos, Á. Molinero-Fernández, M. Á. López, B. Jurado-Sánchez, A. Escarpa, *Anal. Chem.* **2022**, *94*, 5575.
[41] D. Kagan, S. Campuzano, S. Balasubramanian, F. Kuralay, G. U. Flechsig, J. Wang, *Nano Lett.* **2011**, *11*, 2083.
[42] B. Jurado-Sánchez, S. Sattayasamitsathit, W. Gao, L. Santos, Y. Fedorak, V. V. Singh, J. Orozco, M. Galarnyk, J. Wang, *Small* **2014**, *11*, 499.
[43] J. Li, V. V. Singh, S. Sattayasamitsathit, J. Orozco, K. Kaufmann, R. Dong, W. Gao, B. Jurado-Sanchez, Y. Fedorak, J. Wang, *ACS Nano* **2014**, *8*, 11118.
[44] M. Uygun, V. de la Asuncion-Nadal, S. Evli, D. A. Uygun, B. Jurado-Sanchez, A. Escarpa, *Appl. Mater. Today* **2021**, *23*, 101045.
[45] C. C. Mayorga-Martinez, J. Vyskočil, F. Novotný, M. Pumera, *J. Mater. Chem. A* **2021**, *9*, 14904.
[46] C. C. Mayorga-Martinez, J. G. S. Moo, B. Khezri, P. Song, A. C. Fisher, Z. Sofer, M. Pumera, *Adv. Funct. Mater.* **2015**, *26*, 6662.
[47] V. V. Singh, F. Soto, K. Kaufmann, J. Wang, *Angew. Chem.* **2015**, *127*, 7000.
[48] X. Z. Chen, M. Hoop, F. Mushtaq, E. Siringil, C. Hu, B. J. Nelson, S. Pané, *Appl. Mater. Today* **2017**, *9*, 37.
[49] M. Sun, C. Tian, L. Mao, X. Meng, X. Shen, B. Hao, X. Wang, H. Xie, L. Zhang, *Adv. Funct. Mater.* **2022**, *32*, 2112508.
[50] B. Esteban-Fernández de Ávila, P. Angsantikul, D. E. Ramírez-Herrera, F. Soto, H. Teymourian, D. Dehaini, Y. Chen, L. Zhang, J. Wang, *Sci. Robot.* **2018**, *3*, eaat0485.
[51] J. Li, P. Angsantikul, W. Liu, B. Esteban-Fernández de Ávila, X. Chang, E. Sandraz, Y. Liang, S. Zhu, Y. Zhang, C. Chen, W. Gao, L. Zhang, J. Wang, *Adv. Mater.* **2018**, *30*, 1704800.

[52] J. Orozco, G. Pan, S. Sattayasamitsathit, M. Galarnyk, J. Wang, *Analyst* **2015**, *140*, 1421,.
[53] F. Zhang, Z. Li, L. Yin, Q. Zhang, N. Askarinam, R. Mundaca-Uribe, F. Tehrani, E. Karshalev, W. Gao, L. Zhang, J. Wang, *J. Am. Chem. Soc.* **2021**, *143*, 12194.
[54] J. Shim, L. Williams, D. Kim, . Ko, M.-S. Kim, *J. Microbiol. Biotechnol.* **2021**, *31*, 1323.
[55] S. L. Moura, M. Martì, M. I. Pividori, *Sensors* **2020**, *20*, 965.
[56] B. A. Evans, J. C. Ronecker, D. T. Han, D. R. Glass, T. L. Train, A. E. Deatsch, *Mater. Sci. Eng., C* **2016**, *62*, 860.
[57] T. O. Tascì, P. S. Herson, K. B. Neeves, D. W. M. Marr, *Nat. Commun.* **2016**, *7*, 10225.
[58] X. Qiab, Z. Wang, R. Luc, J. Liu, Y. Li, Y. Chen, *Food Chem.* **2020**, *338*, 127837.
[59] Y. Chen, Y. Xianyu, Y. Wang, X. Zhang, R. Cha, J. Sun, X. Jiang, *ACS Nano* **2015**, *9*, 3184.
[60] J. Dai, S. Wu, J. Huang, Q. Wu, F. Zhang, J. Zhang, J. Wang, Y. Ding, S. Zhang, X. Yang, T. Lei, L. Xue, H. Wu, *Front. Microbiol.* **2019**, *10*, 641.
[61] Compliance Policy Guide, Guidance for FDA Staff, https://www.fda.gov/media/77760/download (accessed: September, 2022).